processes

MDPI

Article

Static and Dynamic Simulation of Single and Binary Component Adsorption of CO_2 and CH_4 on Fixed Bed Using Molecular Sieve of Zeolite 4A

Supatsorn Parinyakit [1] and Patcharin Worathanakul [1,2,*]

[1] Department of Chemical Engineering, Faculty of Engineering, King Mongkut's University of Technology North Bangkok, 1518 Pracharat 1, Wongsawang, Bangsue, Bangkok 10800, Thailand; momaysupatsorn@hotmail.com

[2] Center of Eco-Materials and Cleaner Technology (CECT), Science and Technology Research Institute, King Mongkut's University of Technology North Bangkok, 1518 Pracharat 1, Wongsawang, Bangsue, Bangkok 10800, Thailand

* Correspondence: patcharin.w@eng.kmutnb.ac.th; Tel.: +66-2913-2500 (ext. 8242)

Abstract: The simulation of carbon dioxide (CO_2)-methane (CH_4) mixed gas adsorption and the selectivity on zeolite 4A using Aspen Adsorption were studied. The influence of temperature ranging from 273 to 343 K, pressure up to 10 bar and various compositions of CO_2 in the binary system were simulated. The findings of the study demonstrate that the models are accurate. In addition, the effects of various key parameters such as temperature, pressure, and various compositions of binary gases were investigated. The highest CO_2 and CH_4 adsorption are found at 273 K and 10 bar in the Langmuir isotherm model with 5.86 and 2.88 mmol/g, respectively. The amount of CO_2 adsorbed and the selectivity of the binary mixture gas depends on the composition of CO_2. The kinetics of adsorption for pure components of CO_2 at high temperatures can reach saturation faster than CH_4. The influence of the physical properties of zeolite 4A on kinetic adsorption were also studied, and it was observed that small adsorbent particles, large pore diameter, and large pore volume would enter saturation quickly. The prediction of CO_2-CH_4 mixed gas adsorption and selectivity on zeolite 4A were developed for further use for commercial gas separation.

Keywords: adsorption; simulation; carbon dioxide; methane; Aspen Adsorption

Citation: Parinyakit, S.; Worathanakul, P. Static and Dynamic Simulation of Single and Binary Component Adsorption of CO_2 and CH_4 on Fixed Bed Using Molecular Sieve of Zeolite 4A. *Processes* **2021**, *9*, 1250. https://doi.org/10.3390/pr9071250

Academic Editors: Sebastián Sánchez Villasclaras and Federica Raganati

Received: 16 May 2021
Accepted: 16 July 2021
Published: 20 July 2021

1. Introduction

Carbon dioxide (CO_2) and methane (CH_4) are the main components of greenhouse gases that affect global warming. CO_2 emissions primarily involve the burning of fossil fuels [1]. Therefore, carbon dioxide trapping and storage also reduces CO_2 emissions into the atmosphere, and the stored CO_2 can be used for various benefits. The purity of CO_2 is often used directly in the food industry and enhanced oil recovery. There are new chemical and biological transformations of CO_2 into a feedstock for the manufacturing of chemicals and materials such as organic chemistry, minerals, and polymers. Conversion of CO_2 into polymers is one of the added value methods for CO_2 applications, CO_2 is used to copolymerize with various monomers [2]. Therefore, improving the purity of CO_2 from the burning of fossil fuels through various processes is important. Improving of CH_4 purity produced from natural gas, fermenting organic matter, and coal and natural gas refining by removing contaminant gases such as CO_2, O_2, N_2, H_2S, and H_2O is also important. Pure CH_4 is important for industries such as pulp and paper manufacturing, food processes, and petroleum refineries. In addition, CH_4 is an ingredient in various materials such as, fabric, antifreeze, and fertilizer [3]. The purity of CO_2 and CH_4 can be accomplished effectively through pressure swing adsorption (PSA) or temperature swing adsorption (TSA).

The CO_2 and CH_4 gas separation process can be performed through various methods, including distillation, extraction, membrane separation, and adsorption [4–7]. The chemical

industry realized the sustainable development of new innovative processes that use energy and materials more efficiently, since separation processes are of great economic importance accounting for 40–60% of operating costs in the industry. Therefore, a separation process must be developed to save energy consumption and costs. Gas separation by adsorption technology with effective adsorbents is the most common method in the chemical industry [8]. The adsorption process of the components of a fluid mixture flowing through the packed bed of an adsorbent porous material with a large surface area must be considered for proper separation. Different characteristics of the adsorbent influence their applications and these characteristics are influenced by the preparation methods. The most common adsorbents used for the purification of CO_2/CH_4 purposes are activated carbon, alumina, silica gel, and zeolites [9–12]. This research chose the adsorbent zeolite because of its high surface area and high adsorption capacity.

Zeolites are crystalline aluminosilicates of alkaline metals, alkaline earth metals, or other cations with various porous characteristics [13]. Zeolites can be used for a variety of applications depending on the pore structure and the properties of each type of zeolite. They can be used for separation or purification gas processes because of their molecular sieve property. Zeolite has a specific cation for the ion exchange process. Therefore, zeolite is an important adsorbent with specific properties for CO_2 adsorption because of the high adsorbent surface area and the medium and small pores such as synthesized zeolite A, zeolite X, and zeolite Y [14,15].

Moreover, the development in the simulation process is important to help save cost, energy, and time. In addition, it can help to reduce environmental pollution due to the suitable conditions found in the simulation models. Aspen Adsorption is a simulator developed for the design of the adsorption process simulation, covering a wide range of adsorption conditions. Therefore, this research chose Aspen Adsorption for the simulation of the adsorption processes. The molecular simulation of the adsorption processes can also be simulated using GCMC simulation. Chong and Myshakin [16] studied the molecular simulations of the competitive adsorption of the CO_2-CH_4 mixture on illitic clay surfaces under dry conditions, which showed that CO_2 was specially adsorbed on illitic surfaces and possessed the ability to promote methane desorption. The gas mixture adsorption isotherms of CO_2:CH_4 indicated that the CO_2 concentration increase, caused consistent suppression of CH_4 adsorption [16]. However, the adsorption simulation can use mathematical models for prediction breakthrough curves for adsorption. Al Mesfer [17] studied the simulation for CO_2 adsorption from CO_2-N_2 mixture using a packed column on activated carbon, which illustrated that breakthrough time decreased with increasing temperature, feed rate, and increased CO_2 concentration [17]. The experimental results were compared to simulate mathematical models of breakthrough curves with high accuracy [18]. Until now, there were no studies for CO_2 adsorption from CO_2-CH_4 mixed gas using zeolite 4A, which were reviewed.

This computer simulation research through Aspen Adsorption aimed for CO_2 adsorption from CO_2-CH_4 mixed gas using zeolite 4A and the optimum conditions for adsorption. Therefore, the main objectives of this research were to study the factors affecting CO_2 and CH_4 adsorption and the selectivity of binary gas mixtures on zeolite 4A at temperatures ranging from 273 to 343 K, a pressure range of 0–10 bar, and the compositions of CO_2 in the binary system were 10:90, 30:70, 40:60, 50:50, 60:40, and 80:20.

2. Materials and Methods

2.1. Simulation Setting

Data for program modeling included the physical properties of the adsorbent tower, the adsorbent and the conditions of operation. For this research, the adsorbent material was zeolite 4A and CO_2 and CH_4 were adsorbates. The physical properties of the adsorbents and the column for the packing tower are shown in Table 1. The characterization of zeolite 4A and experimental data are from Seabra and coworkers [19]. This research used the results from the experiment of adsorption of pure CO_2 and CH_4 on zeolite 4A at

303 and 343 K to predict the adsorption at 273, 283, and 323 K with the program Aspen Adsorption V11.

Table 1. Physical properties of the zeolite 4A adsorbent and column used in simulation of adsorption.

Parameters	Value
Packing length (mm)	97.5
Internal bed diameter (mm)	9.1
Particle size (cm)	0.2 (average diameter)
Pellet density (kg/m^3)	1109
Solid density of adsorbent (kg/m^3)	2429
Total intrusion volume (cm^3/g)	0.3147
BET surface area (m^2/g)	501.4

The zeolite 4A diameter was in the range of 0.16–0.25 cm in granular form as shown in Table 1. The pellet density and total intrusion volume were obtained by mercury intrusion and the solid density was obtained by helium picnometry. The BET surface area was measured from the N_2 adsorption at 77 K in granule form [19].

Dynamic Simulation of Adsorption Experiments

Dynamic adsorption experiments were simulated by the Aspen Adsorption V11 program. The flow sheet including adsorbent characteristics (gas bed), feed gas, and product streams is shown in Figure 1. The internal diameter bed was 9.1 mm and the packing length was 97.5 mm in the column. The gas bed model configuration allowed for specifying the number of layers, labels for each component and setting the geometry of the bed. There were a set of assumptions for all layers, constant variables, and initial conditions. General assumptions of Aspen Adsorption including partial differential equation (PDE) discretization method were used to approximate spatial derivatives and number PDE nodes with 20 nodes. Material balance was assumed with convection only, momentum balance was laminar, and turbulent flow conditions during operation used the Ergun equation. The kinetic model was set as linear lumped resistance (LDF) and the mass transfer coefficient was constant. The isotherm for the pure components was determined using the Langmuir isotherm. The simulation model was calculated in the multicomponent with an extended Langmuir model based on partial pressure. Energy balance for this research was defined for non-isothermal conditions with no conduction. The heat transfer to the environment was set as adiabatic (no external heat transfer) [20,21].

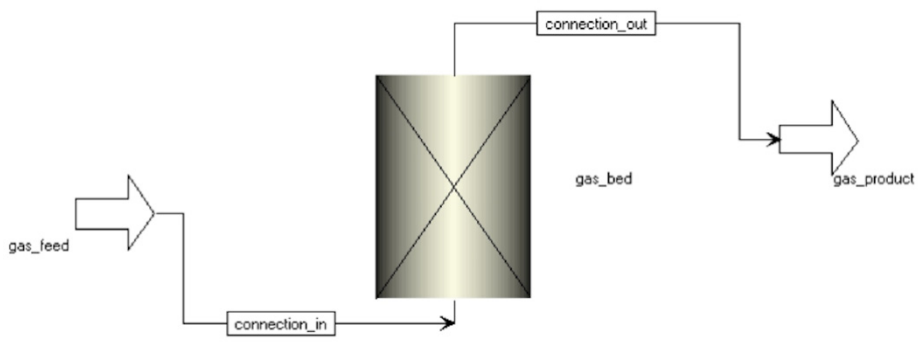

Figure 1. Flowsheet configuration used to run the simulation of adsorption using Aspen Adsorption V11 simulation.

2.2. Adsorption Isotherm Model

2.2.1. Pure Component Adsorption Isotherm

Isotherms of pure CO_2 and CH_4 at 273, 283, 303, 323 and 343 K and pressure ranging from 1 to 10 bar were studied using the Langmuir isotherm model. This simulation was compared to the results of Seabra and coworkers [19].

The Langmuir isotherm model is a replica of the easiest and most popular isotherm model as shown in Equation (1). This model was used for monolayer adsorption and physical adsorption [22].

$$q = \frac{q_m bP}{1 + bP} \tag{1}$$

where q (mmol/g) is the amount adsorbed, q_m (mmol/g) is the maximum adsorption capacity of the adsorbent, P (bar) is the pressure and b (bar^{-1}) is the Langmuir constant. The Langmuir constant depends on the temperature of the system, represented by Equation (2).

$$b = b_0 e^{\frac{-\Delta H}{RT}} \tag{2}$$

where b_0 (bar^{-1}) is the adsorption constant at an infinite temperature, $-\Delta H$ (J/mmol) is the heat of adsorption, R (J·K^{-1}·mol^{-1}) is the universal gas constant, and T (K) is the temperature of the system.

2.2.2. Binary Component Adsorption Isotherm

Adsorption equilibrium for the binary gas mixture between CO_2 and CH_4 was predicted. The temperatures were at 273, 283, 303, 323, and 343 K with pressure ranging from 1 to 10 bars. The compositions of CO_2 to CH_4 were 10:90, 30:70, 40:60, 50:50, 60:40, and 80:20 using an extended Langmuir (EL) isotherm model and the ideal adsorbed solution theory (IAST). The extended Langmuir isotherm model for a binary component or multi-component adsorption was developed from the Langmuir model. In pure components, EL used the information of adsorption from Equation (3) [23].

$$q_i = \frac{q_{m,i} b_i P_i}{1 + \Sigma b_i P_i} \tag{3}$$

where q_i (mmol/g) is the amount adsorbed of component i, q_m (mmol/g) is the maximum adsorption capacity of the adsorbent of component i, P_i (bar)is the partial pressure of component i and b (bar^{-1}) is the Langmuir constant of component i. Therefore, the EL model for binary components is shown in Equations (4) and (5).

For binary component:

$$q_1 = \frac{q_{m,1} b_1 P_1}{1 + b_1 P_1 + b_2 P_2} \tag{4}$$

$$q_2 = \frac{q_{m,2} b_2 P_2}{1 + b_1 P_1 + b_2 P_2} \tag{5}$$

IAST is used to predict the adsorption capacity of binary mixed gas using pure component data. IAST is a thermodynamic method based on the adsorption equilibrium with Raoult's law for vapor-liquid equilibrium. The equilibrium between adsorbed phase and ideal gas phase can be specified by Equation (6) [24–26].

$$Py_i = P_i^0(\pi^*) x_i \tag{6}$$

where y_i and x_i are the molar fractions of component i in the gas phase and adsorbed phase, respectively. P (bar) is the total pressure of the mixture, and $P_i^0(\pi^*)$ (bar) is the equilibrium gas phase pressure of pure component i corresponding to solution temperature and solution spreading pressure, π*.

For a pure component i, the spreading pressure using Equations (7) and (8) was followed:

$$\pi^* = \frac{\pi_i A}{RT} = \int_0^{P_i^0} \frac{q_i}{Pi} dP_i \tag{7}$$

where π_i* is the reduced spreading pressure of component i in the adsorbed phase, π_i is the spreading pressure of component i in the adsorbed phase, A is the specific surface area of the adsorbent, q_i is the pure component adsorption isotherm equation, and P_i^0 is

the standard state pressure of pure component i corresponding to spreading pressure of the mixture.

At the standard state, reduced spreading pressure of the mixture (π*) is the same as the reduced spreading pressure of a single component according to Equation (8).

$$\pi_1^* = \pi_2^* = \ldots = \pi^* \tag{8}$$

For binary mixtures, Equations (6)–(8) were solved numerically and the total adsorbed amount was calculated by Equations (9)–(11).

$$\frac{1}{q_T} = \frac{x_1}{q_1(p_1^0)} + \frac{x_2}{q_2(p_2^0)} \tag{9}$$

$$x_1 + x_2 = 1 \tag{10}$$

$$q_i = x_i q_T \tag{11}$$

where q_T (mmol/g) is the total amount adsorbed.

2.3. Modeling of Mass Transfer Coefficient

Mass transfer coefficients (MTC) were shown in Equation (12) which was assumed to be constant. MTC included the effects of micropore, macropore and film resistances [27]. The effect of macropore was considered using the following equation.

$$k_i = \frac{15\varepsilon_p D_{pi}}{R_p^2} \tag{12}$$

where k_i (s^{-1}) is the overall mass transfer coefficient of species i, D_{pi} (cm^2/s) is the macropore diffusivity of species i, and R_p (cm) is the particle radius and ε_p is the porosity of adsorbent particle or intraparticle.

The effective macropore diffusivity can be determined using the Bosanquet equation [28]:

$$\frac{1}{D_{pi}} = \tau\left(\frac{1}{D_{ki}} + \frac{1}{D_{mi}}\right) \tag{13}$$

where τ is the pore tortuosity factor, D_{ki} (cm^2/s) is the Knudsen diffusivity and D_{mi} (cm^2/s) is the molecular diffusivity.

Estimation of the molecular diffusivity of binary gas mixtures with the best method calculated from the Lennard-Jones equation represented using Equation (14) [28]. The molecular diffusivity was determined using the following equation.

$$D_m = \frac{0.001858T^{\frac{3}{2}}}{P\sigma_{12}^2\Omega_D}\left\{\frac{1}{M_1} + \frac{1}{M_2}\right\} \tag{14}$$

where M_i (g/mol) is the molecular weight of species i, Ω_D is the collision integral and σ_{12} (Å) is the collision diameter of the binary pair of species A and B.

Knudsen diffusion is gas diffusion through small pores, which can be calculated using Equation (15).

$$D_{k_i} = 9700R_P\sqrt{\frac{T}{m_i}} \tag{15}$$

where R_P (cm) is pore radius.

2.4. Selectivity of CO_2 over CH_4 in Binary Mixture Gas

Selectivity represents the ratio of the amount of adsorption of the two gases. It can also be called separation coefficient. If the selectivity of CO_2/CH_4 is high, it means that the adsorption amount of CO_2 is greater than CH_4 [10].

The adsorption selectivity of CO_2 over CH_4 in binary mixtures was defined in Equation (16).

$$S_{CO_2/CH_4} = \frac{\frac{q_{CO_2}}{q_{CH_4}}}{\frac{P_{CO_2}}{P_{CH_4}}} \tag{16}$$

where q_{CO_2} and q_{CH_4} (mmol/g) are the amount adsorbed of CO_2 and CH_4, and P_{CO_2} and P_{CH_4} (bar) are the partial pressures of CO_2 and CH_4, respectively.

2.5. Breakthrough Curves Modeling

To assess the performance of the fixed-bed adsorption column and measure the breakthrough curves, it is necessary to design and utilize the lab-scale experimental setup. By optimizing the mathematical models to the measured experimental data, the useful information can be used to design large-scale industrial columns and to predict the practical conditions. The model used in this work are the Thomas model and the Yoon–Nelson model.

2.5.1. Thomas Model

The Thomas model [29] is one of the most commonly used in the prediction of the breakthrough curve and the describing of the column performance. This model was developed based on the Langmuir kinetics of adsorption that assumed negligible axial dispersion in the column adsorption. The rate of the driving force carries out the second-order reversible reaction kinetics [30]. The Thomas model is shown in Equation (17):

$$\frac{C}{C_0} = \frac{1}{1 + \exp\left(\frac{k_{Th} q_0 M}{Q} - k_{Th} C_0 t\right)} \tag{17}$$

where q_0 is the equilibrium adsorbate uptake in adsorbent (mg/g), Q is the flow rate (mL/min), M is the mass of the adsorbent (g), C is effluent concentration (mg/L), C_0 is influent concentration (mg/L), t is time (min), and k_{Th} is the Thomas model constant (mL/min·mg).

2.5.2. Yoon-Nelson Model

The Yoon-Nelson model [31] is based on the assumption that the rate of decrease in the probability of adsorption for each adsorbate is proportional to the probability of adsorbate breakthrough on the adsorbent [32]. The Yoon-Nelson model was used for the following equation.

$$\frac{C}{C_0} = \frac{\exp(k_{YN} t - \tau k_{YN})}{1 + \exp(k_{YN} t - \tau k_{YN})} \tag{18}$$

where k_{YN} is the Yoon-Nelson constant (min^{-1}) and τ is the time required to reach the effluent concentration to 50% of the influent concentration (min).

3. Results and Discussion

3.1. Pure Component Adsorption Isotherm

Adsorption isotherm of pure CO_2 and pure CH_4 at different temperatures and pressures are shown in Figure 2. The experimental data for pure CO_2 and CH_4 adsorption at 303 and 343 K were from Seabra [19]. The experimental results are fitted with the Langmuir isotherm model in Equations (1) and (2).

The adsorption capacity of CO_2 and CH_4 decreased with the rising temperature, indicating the adsorption of CO_2 and CH_4 are exothermic physical. The type of physical and chemical adsorption depends on the amount of heat in the adsorption. For heat of adsorption with 80 kJ·mol^{-1} or more, the adsorption process indicates chemisorption, while lower values represent a physical adsorption [33]. Values of the isosteric heat of adsorption in zeolite 4A of 47.8 kJ mol^{-1} for the adsorption of CO_2 [34] and 16.72 kJ·mol^{-1} for CH_4 [35] were found. Thus, the adsorption of CO_2 and CH_4 on zeolite 4A was physical adsorption;

it could adsorb well when the temperature is decreased. In fact, as temperature decreases, gas molecules have less kinetic energy because the bond between gas and adsorbent is increased [36,37]. Moreover, the effect of pressure on the adsorption capacity is shown in Figure 2. The adsorption capacity increased rapidly as the pressure increased due to an increase in the gas molecules hitting the surface. Therefore, the increase in pressure caused the adsorption rate to increase linearly. However, when the pressure became high and almost the entire surface of the adsorbent received saturated gas, the pressure had little effect on the adsorption capacity. Ultimately, it could reach a point where the pressure did not affect the adsorption capacity because the number of adsorption sites was fixed, and no more adsorption occurred in those sites. At the same pressure and temperature conditions, the adsorption capacity of CO_2 is much higher than CH_4 because CO_2 has a quadrupole moment and polarizability greater than CH_4, and it also has a high critical temperature as shown in Table 2 [38,39].

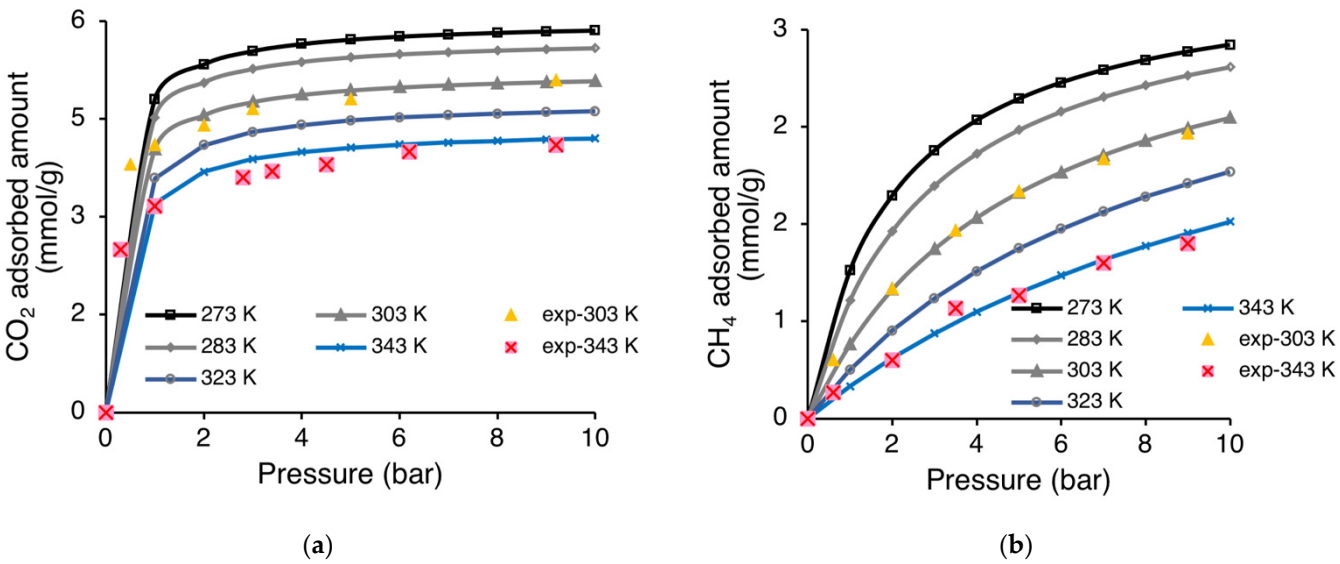

(**a**) (**b**)

Figure 2. Adsorption isotherm on zeolite 4A at different temperatures and pressures: (**a**) pure CO_2; (**b**) pure CH_4.

Table 2. Properties of carbon dioxide and methane.

Properties	CO_2	CH_4
Kinetic diameter (Å)	3.3	3.8
Critical temperature (K)	304.12	190.56
Quadrupole moment ($\times 10^{26}$ esu cm^2)	4.30	0
Polarizability ($\times 10^{-25}$ cm^3)	29.11	25.93

Table 3 shows the parameters of the Langmuir isotherm model for CO_2 and CH_4 adsorption on zeolite 4A. Where $q_{m,0}$ is maximum adsorption capacity, b_0 is Henry law constant, Q/R is adsorption heat and X is empirical constant. The constant values in Table 3 were used in the Langmuir isotherm model in Equations (1) and (2).

Table 3. Parameters of the Langmuir isotherm model for CO_2 and CH_4 adsorption on zeolite 4A.

Equation	Parameters	CO_2	CH_4
$q = \frac{q_m bP}{1+bP}$	$q_{m,0}$ (mmol/g)	3.7881	3.4698
$b = b_0 e^{\frac{Q}{RT}}$	b_0 (bar^{-1})	0.7078	5.88×10^{-5}
$q_m = q_{m,0} \exp\left(X\left(1 - \frac{T}{T_0}\right)\right)$	Q/R (K)	470.91	2465.8
	X (dimensionless)	1.7188	0.003
	RMS (dimensionless)	0.0915	0.0236

Parameters of the previously mentioned equations were determined by minimizing the root-mean-square (RMS) in Equation (19):

$$\mathrm{RMS} = \left(\frac{\sum_{i=1}^{N} \left(q_i^{cal} - q_i^{exp} \right)^2}{N} \right)^{0.5} \tag{19}$$

where N is the number of data points and q_i^{cal} and q_i^{exp} are calculated and experimental adsorbed amounts, respectively. Low RMS value indicates that the Langmuir isotherm model is suitable.

The Langmuir isotherm model depends on pressure, maximum adsorption capacity of the adsorbent, and the Langmuir constant. Maximum adsorption capacity and the Langmuir constant depend on temperature. Therefore, the amount of adsorption for each pressure and temperature could be determined [22].

The crystal structure of zeolite 4A with sodium cation distribution as shown in Figure 3. There are three sites for sodium cation distribution including site I (S1) at the center of the 6-rings of sodalite cages, site II (S2) at the center of the 8-ring window of α cages and site III (S3) at opposite the 4-rings on the interior of α cages. Sodium ions in zeolite 4A contains 12 ions per unit cell (S1:S2:S3 = 8:3:1) [40,41].

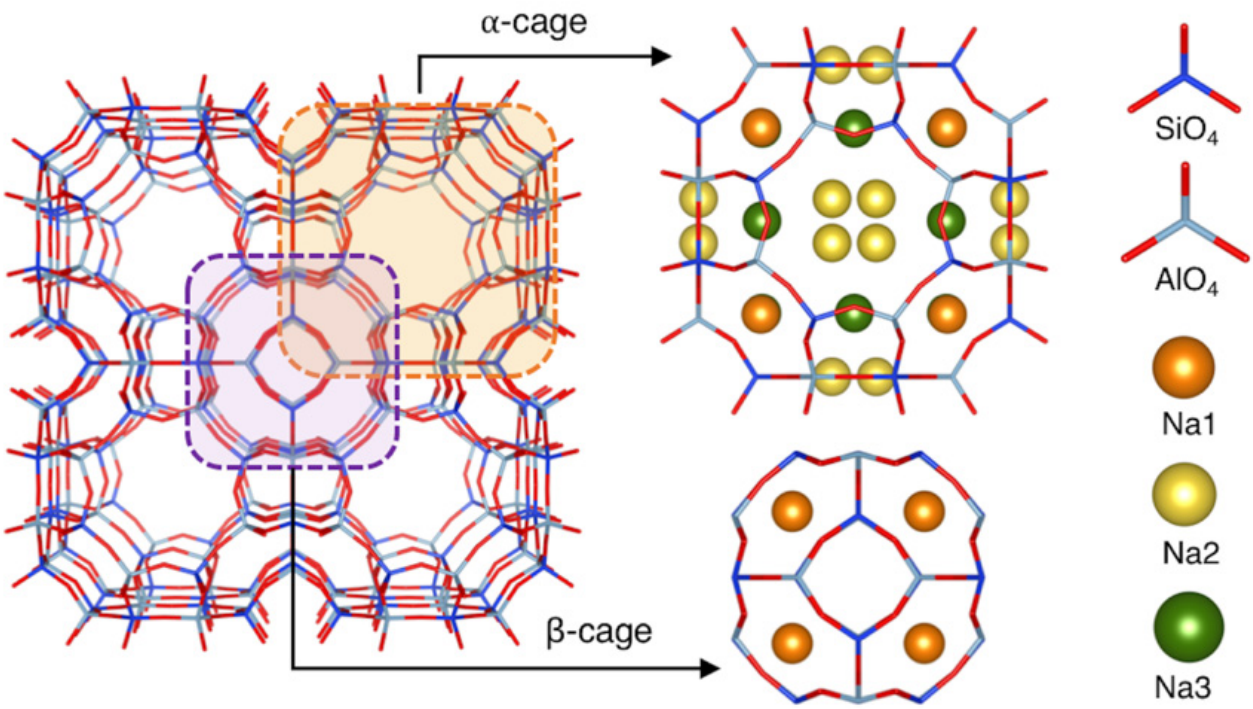

Figure 3. The crystal structure of zeolite 4A.

The adsorption mechanism of the CO_2 molecule on zeolite 4A showed that CO_2 interacts with the sodium cations in the adsorption site. Interaction between the CO_2 quadrupole and sodium cations was electrostatic interaction. Sites of CO_2 adsorption interaction with the sodium cation were shown in a single cation site. CO_2 interacted with two sodium cations at dual cation sites. Moreover, CO_2 could interact with more than two sodium cations and was denoted as multiple cation sites [42,43]. For instance, interaction between CO_2 and zeolite 4A was shown in Figure 4. The CO_2 molecule interacted with the sodium cation in S1 perpendicular to the plane of the 6-rings of sodalite cages along the body diagonal. If the distance between the CO_2 molecule and sodium cation is long distance, it indicates a weak interaction.

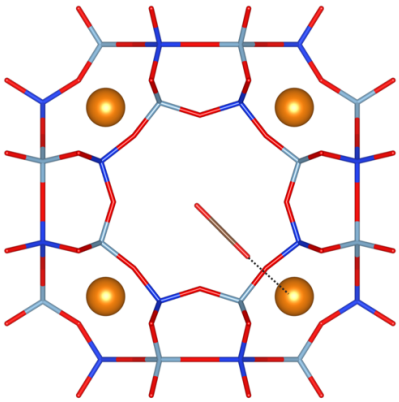

Figure 4. Interaction between CO_2 and zeolite 4A.

Likewise, CH_4 interacted with sodium cation the same as CO_2. However, the distance or molecular arrangement may differ due to the different properties of CO_2 and CH_4 as shown in Table 2. The CH_4 has zero quadrupole moment and polarizability less than CO_2. Therefore, the electrostatic affinity and adsorption capacity for CH_4 were less than CO_2. For the distance between the gas molecule and the cation, the longer distance indicated a weak interaction. In addition, CO_2 and CH_4 molecules could interact with oxygen atoms of the framework as well.

3.2. Binary Component Adsorption Isotherm

The simulation was predicted for a binary gas mixture using extended Langmuir Equations (4) and (5) and the ideal adsorbed solution theory models used in Equations (9)–(11). The composition of CO_2 and CH_4 in the gas mixture affected the amount of adsorption. The predictions of the adsorption of the binary gas mixture between CO_2 and CH_4 on zeolite 4A with the EL isotherm model were shown in Figure 5a,b.

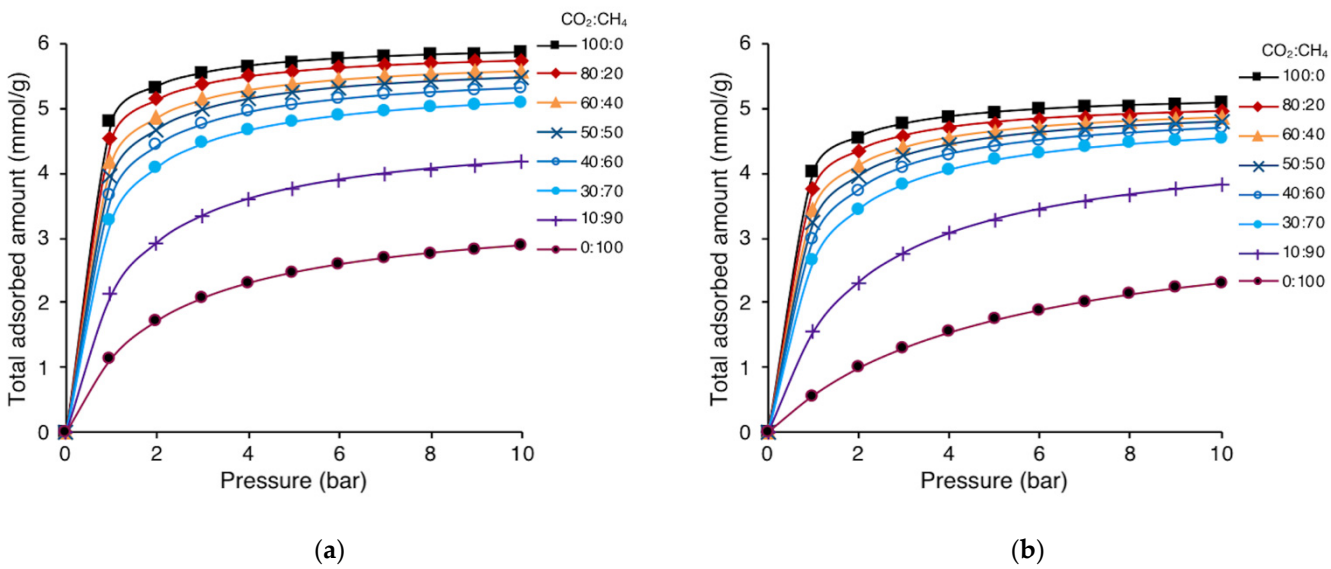

Figure 5. Adsorption isotherm of CO_2-CH_4 mixture on zeolite 4A with the EL isotherm model at different temperatures: (**a**) 273 K and (**b**) 303 K.

The results showed that the total amount of adsorbed gas mixture increased with the amount of CO_2 adsorption. In other words, the higher the composition of CO_2 received the greater the amount of total gas adsorption. Thus, the adsorption capacity of the mixed gas was between the two pure gases due to gas mixture had competition and was a hinderance between CO_2 and CH_4 molecules in the adsorption. It was indicated that the quadrupole

moment of CO_2 could result in strong interactions between CO_2 molecules and the surface of zeolite 4A. The effect of pressure and temperature on the adsorption of the binary gas mixture showed the same tendency as the pure component [44–46]. Therefore, the adsorption of the mixed gas was also a physical adsorption because the total amount adsorbed decreased with the rising temperature.

Zeolite 4A has a cubic structure as shown in Figure 3. The effective size of its windows depends on the sodium cation of zeolite 4A, which has a pore window size of approximately 0.38 nm. The kinetic diameter affected the separation of CO_2 from CH_4 as observed in theory. These pores of zeolite have dimensions very close to the kinetic diameters of CO_2 and CH_4, allowing CO_2 to diffuse through the adsorbent faster than CH_4. Therefore, CO_2 can be separated from CH_4 while CO_2 diffuses more quickly in narrow pores than CH_4 with a kinetic diameter effect. For the molecular sieve effect, both CO_2 and CH_4 have different kinetic diameters inside a zeolite as shown in Table 2. CO_2 has the smallest kinetic diameter at 0.33 nm, and CH_4 at 0.38 nm. Zeolite 4A showed pore window apertures that are similar to the kinetic diameter of CH_4. Therefore, CO_2 could enter the zeolite 4A freely, but CH_4 was blocked [47].

Figure 6 showed the comparison between the EL and IAST models of the CO_2-CH_4 mixture in different CO_2 and CH_4 ratios. The total adsorption of IAST is a little higher than the EL model. The total adsorption between IAST and EL models was approximately the same. The IAST model showed better adsorption of the CO_2-CH_4 gas mixture than the EL model compared to the experimental results according to the study of Rios [48]. In Wu's research [39], IAST could be used to predict the behavior of a binary mixture with very high accuracy. The IAST model was able to work very well when the adsorbates were similar sizes. On the other hand, the EL model was able to predict sorption behavior with acceptable precision.

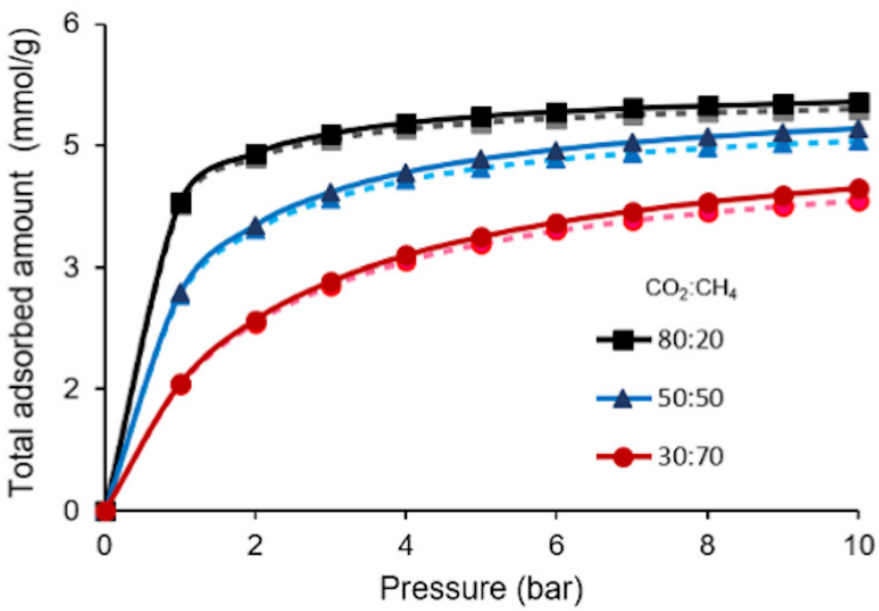

Figure 6. Adsorption isotherm of CO_2-CH_4 mixture on zeolite 4A at 303 K with different models for EL (dash line) and IAST (solid line).

3.3. Selectivity for Separating of CO_2-CH_4 Mixture

The selectivity of binary gas mixtures can be calculated from Equation (16). The selectivity at different compositions of CO_2:CH_4 and pressures shown in Figure 7a at 303 K. If the composition of CO_2 increased, the selectivity also increased because the interaction of CO_2 molecules with the atoms of the zeolite 4A structure was stronger than that with CH_4 molecules. In addition, CO_2 molecules particularly adsorbed well in the pores of zeolite 4A and hindered the diffusion of the weaker adsorbing CH_4 molecules.

The obtained selectivity from IAST and EL models for different compositions are shown in Figure 7a. It was indicated that the EL selectivity of CO_2/CH_4 was constant for all gas compositions and pressures. On the other hand, the IAST selectivity showed various results for both total pressure and composition. From this prediction of IAST, the composition of CO_2 would affect selectivity when the pressure was increased. Figure 7b shows the different temperatures on selectivity of 50:50 of CO_2:CH_4 ratio, at 1 bar. The selectivity increased with rising temperature [49] which is the same in both models. For this reason, the pressure and temperature had a positive impact on the adsorption selectivity of CO_2 over CH_4. Therefore, to predict the selectivity of CO_2-CH_4, the IAST calculation was based on Langmuir and EL calculations.

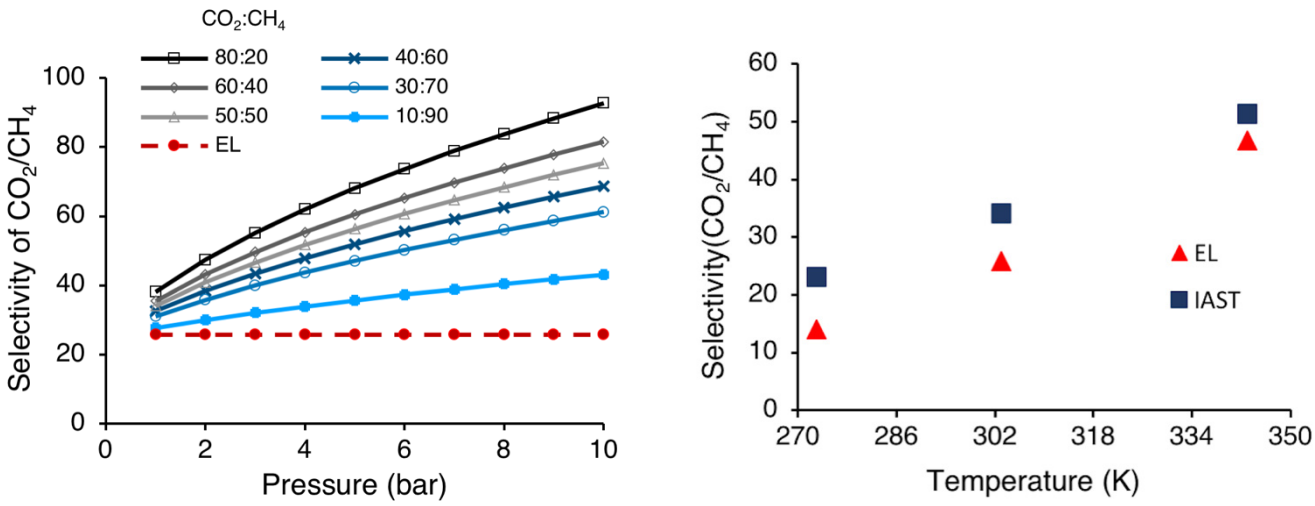

(**a**) (**b**)

Figure 7. The adsorption selectivity of CO_2-CH_4 mixture on zeolite 4A: (**a**) at different pressures and compositions and 303 K (solid line is IAST based on a Langmuir isotherm and dash line is EL isotherm); (**b**) at difference temperature, 1 bar and 50:50 of CO_2:CH_4 ratio.

As mentioned above, the use of an adsorbent must be considered for high efficiency separation. Therefore, the comparison of the adsorption capacity in each adsorbent can be used as analytical data for improving the adsorbent.

Table 4 shows the adsorption capacity for the CO_2-CH_4 binary gas mixture with zeolite compared to others. It can be seen that the adsorption values of both CO_2 and CH_4 from zeolite 4A showed similar trends to those of 13 X and 5A zeolites at the same conditions. The BET specific surface area of zeolite 4A was close to that of zeolite 13X. Therefore, the adsorption capacities of CO_2 were similar to CH_4. There were no different adsorption effects in each zeolite in Table 4. The adsorption capacity of CO_2 showed greater than CH_4. The selectivity of the binary gas mixture has an important parameter because it can form zeolite into an ideal material adsorbent for CO_2 and CH_4 mixture gas separation.

Table 4. Comparison of the adsorption capacity for CO_2-CH_4 binary gas mixture with different adsorbents at 323 K.

Adsorbent	P (Bar)	CO_2:CH_4	q_{CO_2} (mmol/g)	q_{CH_4} mmol/g	Ref.
Zeolite 4A	6	40:60	4.076	0.159	This work
	10	50:50	4.400	0.102	
Zeolite 5A	5.8	40:60	2.852	0.150	[38]
Zeolite 13X	10	50:50	4.277	0.252	[44]

3.4. Dynamic Simulation of Adsorption Experiment

Figure 8 shows the kinetic adsorption of CO_2 and CH_4 on zeolite 4A at different temperatures (273, 303, 343 K) and pressures (1, 5, 10 bar).

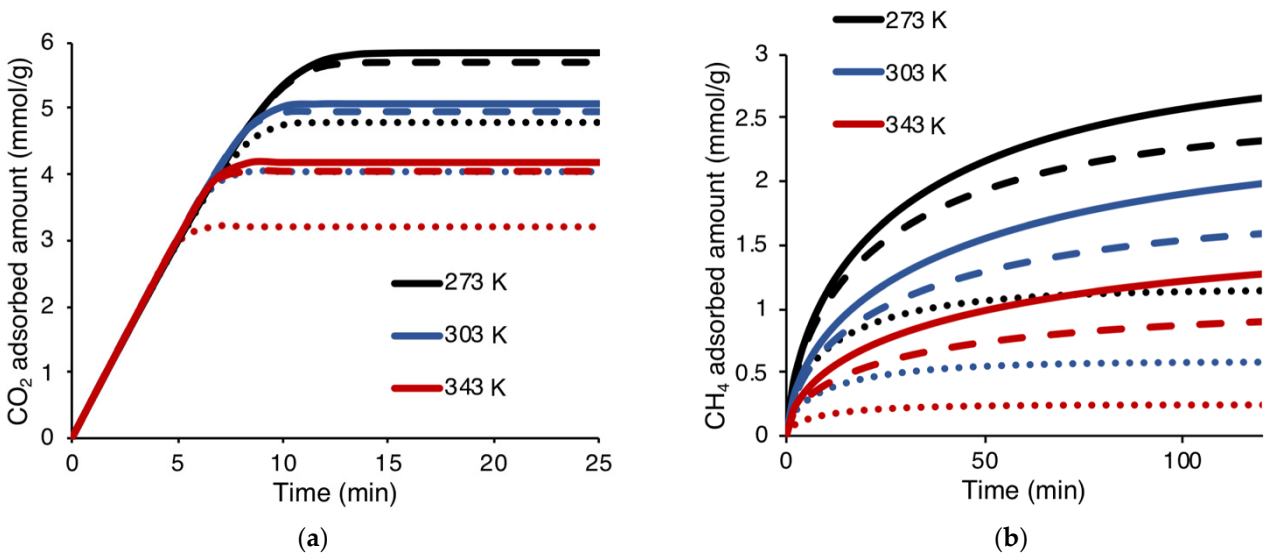

Figure 8. Cumulative adsorbed amount versus time at different temperatures (**a**) CO_2 (**b**) CH_4 with different pressures for 1 bar (round dot), 5 bar (dash line), and 10 bar (solid line).

It was observed that at the beginning of the adsorption, the amount of CO_2 adsorbed on the adsorbent was slightly fast and then slowly decreased until it reached equilibrium. In the initial stages, CO_2 molecules directly contacted with the adsorbent, resulting in great interaction between adsorbate and adsorbent [50]. After total pores were adsorbed without any further adsorption of CO_2 molecules, the process of adsorption went to saturation. In addition, when the temperature increased, faster saturation was observed due to the exothermic process for CO_2 adsorption. In the exothermic process, increasing temperature caused adsorption to decrease because of the decreased of the attraction between the adsorbate and the adsorbent [37,39,44].

The mass transfer coefficient was increased with increased temperature as shown in Table 5. This is caused by CO_2 and CH_4 molecules moving faster with higher temperature from the increased kinetic energy [28,51].

Table 5. Mass transfer coefficient CO_2 and CH_4 adsorption on zeolite 4A (0.2 cm) at different conditions of pressure and temperature.

T (K)	P (Bar)	D_P (cm^2/s)		k (s^{-1})	
		CO_2	CH_4	CO_2	CH_4
273	1	0.0196	0.0386	0.3222	0.6357
	5	0.0046	0.0093	0.0749	0.1524
	10	0.0023	0.0047	0.0382	0.0781
303	1	0.0232	0.0450	0.3820	0.7400
	5	0.0055	0.0102	0.0906	0.1684
	10	0.0030	0.0057	0.0489	0.0942
343	1	0.0283	0.0546	0.4662	0.8985
	5	0.0069	0.0127	0.1137	0.2089
	10	0.0036	0.0071	0.0584	0.1174

From the simulation adsorption model, it was found that pressure affected the adsorption capacity and mass transfer coefficient. The mass transfer coefficient decreased with the rising pressure because of effective diffusivity decreased from decreased molecular dif-

fusion [28,51]. The relation of mass transfer coefficient, effective diffusivity and molecular diffusivity are shown in Equations (12)–(14), respectively. Equation (15) shows Knudsen diffusion which depends on temperature. Figure 8b shows that CH_4 adsorption took a long time to adsorb, due to the decrease in the polarizability and kinetic diameter of CH_4, which was larger than CO_2 as shown in Table 2.

3.4.1. The Effect of the Physical Properties of Zeolite 4A on Kinetic Adsorption

The physical properties of various zeolite 4A with different particle size, pore volume and pore diameter are shown in Table 6. Three types of zeolites were compared in this study: zeolite 4A-0.2 cm, zeolite 4A (HSD, high bulk density)-0.2 cm and zeolite 4A-0.4 cm.

Table 6. Physical properties of zeolite 4A with different types.

Type of Zeolite	Particle Size (cm)	Pore Volume (cm^3/g)	Pore Diameter (nm)	BET Surface (m^2/g)
Zeolite 4A-0.2 cm	0.2	0.3147	361	501.4
Zeolite 4A (HSD)-0.2 cm	0.2	0.1606	320	509.8
Zeolite 4A-0.4 cm	0.4	0.3012	314	510.4

To study the physical properties of the zeolite 4A adsorbents, the model developed to predict the breakthrough curves of CO_2 and CH_4 adsorptions on zeolite 4A was shown in Figure 9. It was found that small particle sizes of zeolite went into saturation and balance more quickly than large ones because of long diffusion inside the pores [52]. For different pore volumes with the same particle size, at large pore volumes could go into saturation quickly because the adsorption capacity was greater for larger pore volumes. Moreover, after all the pores were occupied by the adsorbate, the adsorbent could no longer adsorb CO_2 molecules. The efficiency was high if the amount of porosity was large. Less pore diameter affects the kinetic adsorption on fast diffusion. The effect of pore diameter on the adsorption is mentioned in Section 3.2.

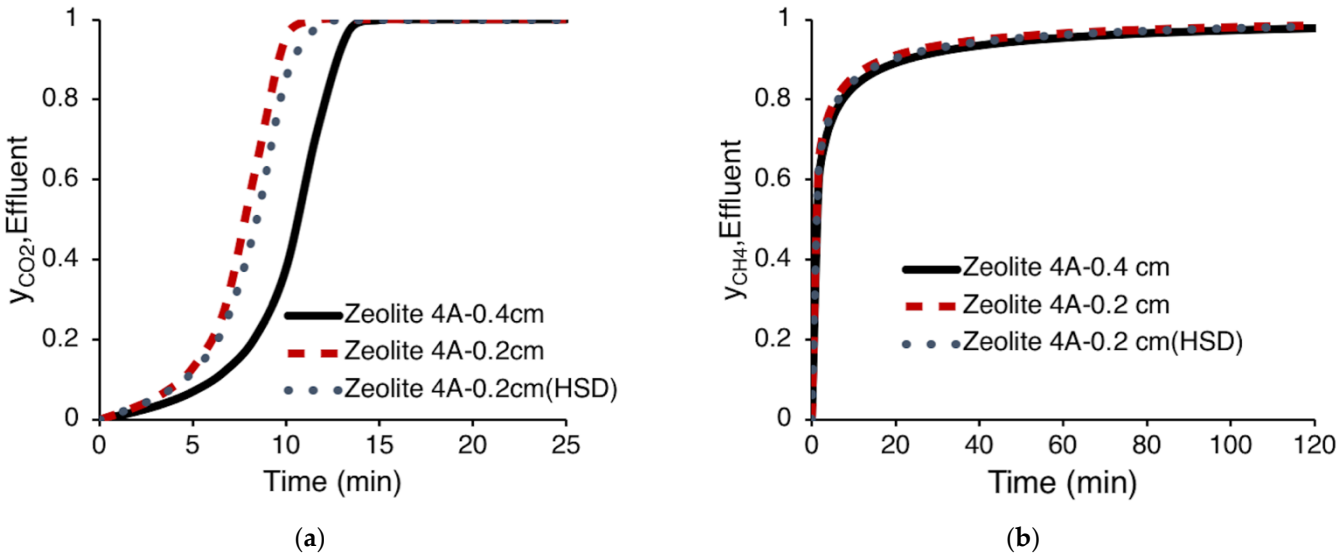

Figure 9. Breakthrough curves on the effect of physical properties of zeolite 4A at 303 K and 10 bar (**a**) CO_2 and (**b**) CH_4.

The mass transfer coefficient of large particles was smaller than the small ones as shown in Table 7. From Equation (12), the mass transfer coefficient was inverse to the particle radius. Therefore, the particle radius was large; the mass transfer coefficient was reduced.

Table 7. Mass transfer coefficients of CO_2 and CH_4 adsorption on different types of zeolites 4A at 303 K and 10 bar.

Type of Zeolite	D_P (cm^2/s)		k(s^{-1})	
	CO_2	CH_4	CO_2	CH_4
Zeolite 4A-0.2 cm	0.0030	0.0057	0.0489	0.0942
Zeolite 4A (HSD)-0.2 cm	0.0028	0.0056	0.0269	0.0546
Zeolite 4A-0.4 cm	0.0028	0.0057	0.012	0.0244

3.4.2. The Effect of Binary CO_2-CH_4 Mixed Gas

Figure 10a,b showed the effect of the composition ratios of CO_2 and CH_4 of 80:20, 50:50 and 30:70 at 303 K and 10 bar pressure.

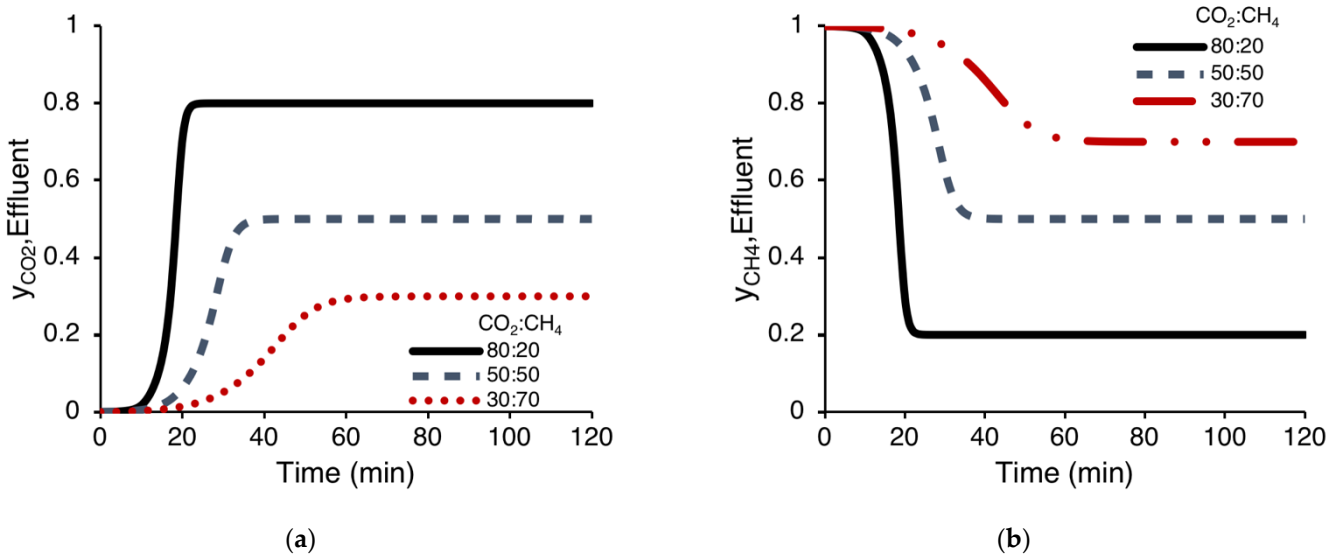

Figure 10. Breakthrough curves on the effect of binary gas mixture on zeolite 4A at 303 K and 10 bar (**a**) CO_2 and (**b**) CH_4.

When CO_2 composition increased, the saturation of the breakthrough curve was decreased, representing the faster kinetics of the adsorption process with a high CO_2 content [53]. It was predicted that CO_2 had a higher adsorption with zeolite 4A than CH_4. As a result, when CO_2 composition was high, competition of CO_2 and CH_4 for adsorption was less than with less composition of CO_2 [54,55].

3.4.3. Modeling of Breakthrough Curves

Modeling of the breakthrough curves were obtained from experiments using the Thomas and Yoon-Nelson model. The experimental data of the adsorption of CO_2 on zeolite 4A at 573.15 K and flow rate of 5 L/h were obtained from Tobarameekul [56].

Figure 11 shows the ability of the Thomas and Yoon-Nelson model to predict the experimental breakthrough curves. The prediction of the Yoon-Nelson model is better than Thomas's model. Both models were formed according to the experimental data. The parameters from fitting the different models to experimental breakthrough curves were shown in Table 8. The correlation coefficient (R^2) of the Yoon-Nelson model is greater than that of Thomas.

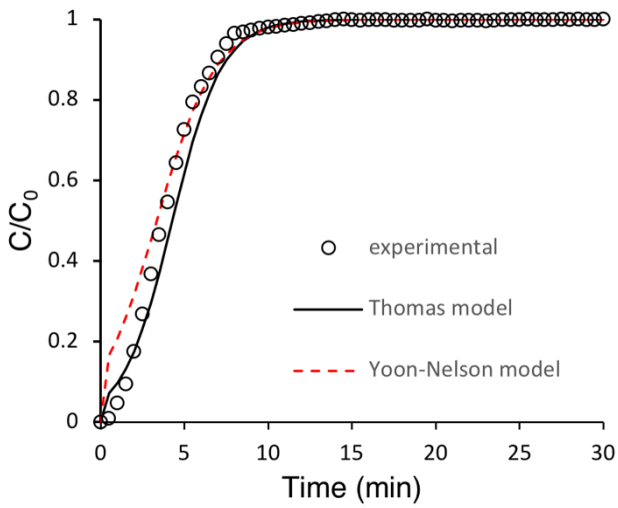

Figure 11. Comparison of the prediction of the Thomas and Yoon-Nelson model with the experimental breakthrough curve.

Table 8. Thomas and Yoon-Nelson model parameters.

Model	Parameter	Value
Thomas	k_{Th} (L/mg min)	1.232×10^{-3}
	q_0 (mg/g)	654,490.9
	R^2	0.948
Yoon-Nelson	k_{YN} (min^{-1})	0.567
	τ (min)	3.347
	R^2	0.974

4. Conclusions

Adsorption isotherms of pure CO_2 and pure CH_4 on zeolite 4A with 273 to 343 K, and pressure up to 10 bar using the Langmuir model were performed. Adsorption generally depended on the temperature. Adsorption decreased with increasing temperature because adsorption processes were exothermic reaction. On the other hand, at a constant temperature, the adsorption capacity increased with pressure. Therefore, the highest CO_2 and CH_4 adsorption from this study was found at 273 K and 10 bar. The properties of CO_2 and CH_4 affected on the adsorption capacity so that the adsorption capacity of CO_2 was much higher than CH_4. The effect of temperature and pressure on the binary gas mixture had the same effect on the pure component of adsorption. However, the adsorption of the mixed gas increased with the amount of CO_2 entered. The effect of pore size on adsorption showed that CO_2 with a smaller kinetic diameter could be separated from CH_4 with a larger kinetic diameter as CO_2 diffuses more quickly in narrow pores than CH_4. In addition, Zeolite 4A has pore window apertures that are similar to the kinetic diameter of CH_4, then CO_2 could enter the zeolite 4A freely, but CH_4 was blocked. Simulation models for gas mixtures were IAST and EL models. The amount of adsorption of the IAST model was greater than the EL model and the selectivity also increased with the amount of CO_2 entered, and the results showed that selectivity rose with the temperature. Moreover, the amount of CO_2 adsorbed from dynamic adsorption simulation increased with increasing pressure because of effective diffusivity decreased from decreased molecular diffusion. At the same time, CH_4 showed the same trend as CO_2, but its adsorption capacity was less than CO_2. In addition, the rising temperature could reach the equilibrium faster than the low temperature. Small adsorbent particles and large pore volume could enter the saturation fast. For the kinetic adsorption simulation of the CO_2-CH_4 binary mixture gas adsorption, the increased composition of CO_2 would greatly benefit the efficiency of CO_2

adsorption in the mixed gas system. Moreover, the prediction of the breakthrough curves from the Yoon-Nelson model was better than Thomas's model.

Author Contributions: Conceptualization, S.P. and P.W.; methodology, S.P. and P.W.; software, S.P.; validation, S.P. and P.W.; formal analysis, S.P. and P.W.; investigation, P.W.; data curation, S.P. and P.W.; writing—original draft preparation, S.P.; writing—review and editing, P.W.; visualization, S.P.; supervision, P.W.; project administration, P.W.; funding acquisition, P.W. Both authors have read and agreed to the published version of the manuscript.

Funding: This research was funded by King Mongkut's University of Technology North Bangkok. Contract no. KMUTNB-63-KNOW-043.

Institutional Review Board Statement: Not applicable.

Informed Consent Statement: Not applicable.

Data Availability Statement: Not applicable.

Conflicts of Interest: The authors declare no conflict of interest.

References

1. Jawaharraj, K.; Shrestha, N.; Chilkoor, G.; Dhiman, S.S.; Islam, J.; Gadhamshetty, V. Valorization of methane from environmental engineering applications: A critical review. *Water Res.* **2020**, *187*, 116400. [CrossRef]
2. Paraschiv, S.; Paraschiv, L.S. Trends of carbon dioxide (CO_2) emissions from fossil fuels combustion (coal, gas and oil) in the EU member states from 1960 to 2018. *Energy Rep.* **2020**, *6*, 237–242. [CrossRef]
3. Qin, Y.; Wang, X. Conversion of CO_2 into Polymers. In *Green Chemistry and Chemical Engineering*; Han, B., Wu, T., Eds.; Springer: New York, NY, USA, 2019; pp. 323–347.
4. Yousef, A.M.; El-Maghlany, W.M.; Eldrainy, Y.A.; Attia, A. Low-Temperature Distillation Process for CO_2/CH_4 Separation: A Study for Avoiding CO_2 Freeze-Out. *J. Heat Transf.* **2017**, *140*. [CrossRef]
5. Qin, C.; Jiang, Y.; Zhou, J.; Song, X.; Liu, Z.; Li, D.; Zhou, F.; Xie, Y.; Xie, C. Effect of supercritical CO_2 extraction on CO_2/CH_4 competitive adsorption in Yanchang shale. *Chem. Eng. J.* **2021**, *412*, 128701. [CrossRef]
6. Zhang, Y.; Sunarso, J.; Liu, S.; Wang, R. Current status and development of membranes for CO_2/CH_4 separation: A review. *Int. J. Greenh. Gas. Control.* **2013**, *12*, 84–107. [CrossRef]
7. Klewiah, I.; Berawala, D.S.; Alexander Walker, H.C.; Andersen, P.Ø.; Nadeau, P.H. Review of experimental sorption studies of CO_2 and CH_4 in shales. *J. Nat. Gas. Sci. Eng.* **2020**, *73*, 103045. [CrossRef]
8. Wankat, P.C. A review of: "Gas Separation Technology". *Sep. Purif. Methods* **1991**, *20*, 199–200. [CrossRef]
9. Álvarez-Gutiérrez, N.; Gil, M.V.; Rubiera, F.; Pevida, C. Adsorption performance indicators for the CO_2/CH_4 separation: Application to biomass-based activated carbons. *Fuel Process. Technol.* **2016**, *142*, 361–369. [CrossRef]
10. Tamnanloo, J.; Fatemi, S.; Golmakani, A. Binary Equilibrium Adsorption Data and Comparison of Zeolites with Activated Carbon for Selective Adsorption of CO_2 from CH_4. *Adsorpt. Sci. Technol.* **2014**, *32*, 707–716. [CrossRef]
11. Zhang, Y.; Chen, K.; Lv, C.; Wu, T.; Wen, Y.; He, H.; Yu, S.; Wang, L. Adsorption Separation of CO_2/CH_4 from Landfill Gas by Ethanolamine-Modified Silica Gel. *WaterAir Soil Pollut.* **2021**, *232*. [CrossRef]
12. Liang, D.; Hu, Y.; Bao, Q.; Zhang, J.; Feng, J.; Sun, P.; Ma, Y.; Zhang, H. A suitable zeolite Rho for separating CO_2/CH_4 in pressure swing adsorption (PSA) process. *Inorg. Chem. Commun.* **2021**, *127*, 108547. [CrossRef]
13. Verma, M.; Kaur, G. A mini review on zeolite. *Mater. Today Proc.* **2021**. [CrossRef]
14. Dusselier, M.; Davis, M.E. Small-Pore Zeolites: Synthesis and Catalysis. *Chem. Rev.* **2018**, *118*, 5265–5329. [CrossRef]
15. Li, Y.; Li, L.; Yu, J. Applications of Zeolites in Sustainable Chemistry. *Chem* **2017**, *3*, 928–949. [CrossRef]
16. Chong, L.; Myshakin, E.M. Molecular simulations of competitive adsorption of carbon dioxide—Methane mixture on illitic clay surfaces. *Fluid Phase Equilibria* **2018**, *472*, 185–195. [CrossRef]
17. Al Mesfer, M.K.; Amari, A.; Danish, M.; Al Alwan, B.A.; Shah, M. Simulation study of fixed-bed CO_2 adsorption from CO_2/N_2 mixture using activated carbon. *Chem. Eng. Commun.* **2020**, 1–10. [CrossRef]
18. Brea, P.; Delgado, J.A.; Águeda, V.I.; Uguina, M.A. Modeling of breakthrough curves of N_2, CH_4, CO, CO_2 and a SMR type off-gas mixture on a fixed bed of BPL activated carbon. *Sep. Purif. Technol.* **2017**, *179*, 61–71. [CrossRef]
19. Seabra, R.; Ribeiro, A.; Gleichmann, K.; Ferreira, A.; Rodrigues, A. Adsorption equilibrium and kinetics of carbon dioxide, methane and nitrogen on binderless zeolite 4A adsorbents. *Microporous Mesoporous Mater.* **2018**, *277*. [CrossRef]
20. Wood, K.; Liu, Y.; Yu, Y. *Simulation of Adsorption Processes*; Wiley: Hoboken, NJ, USA, 2018; pp. 1–153.
21. Plaza, M.G.; Durán, I.; Querejeta, N.; Rubiera, F.; Pevida, C. Experimental and Simulation Study of Adsorption in Postcombustion Conditions Using a Microporous Biochar. 1. CO_2 and N_2 Adsorption. *Ind. Eng. Chem. Res.* **2016**, *55*, 3097–3112. [CrossRef]
22. Azizian, S.; Eris, S. Chapter 6—Adsorption isotherms and kinetics. In *Interface Science and Technology*; Ghaedi, M., Ed.; Elsevier: Amsterdam, The Netherlands, 2021; Volume 33, pp. 445–509.

23. Kapoor, A.; Ritter, J.A.; Yang, R.T. An extended Langmuir model for adsorption of gas mixtures on heterogeneous surfaces. *Langmuir* **1990**, *6*, 660–664. [CrossRef]
24. Goel, C.; Bhunia, H.; Bajpai, P. Prediction of Binary Gas Adsorption of CO_2 /N_2 and Thermodynamic Studies on Nitrogen Enriched Nanostructured Carbon Adsorbents. *J. Chem. Eng. Data* **2017**, *62*, 214–225. [CrossRef]
25. LeVan, M.D.; Vermeulen, T. Binary Langmuir and Freundlich isotherms for ideal adsorbed solutions. *J. Phys. Chem.* **1981**, *85*, 3247–3250. [CrossRef]
26. McIntyre, S.M.; Shan, B.; Wang, R.; Zhong, C.; Liu, J.; Mu, B. Monte Carlo Simulations to Examine the Role of Pore Structure on Ambient Air Separation in Metal–Organic Frameworks. *Ind. Eng. Chem. Res.* **2018**, *57*, 9240–9253. [CrossRef]
27. Hauchhum, S.; Mahanta, P.; De Wilde, J. Capture of CO_2 from Flue Gas onto Coconut Fibre-Based Activated Carbon and Zeolites in a Fixed Bed. *Transp. Porous Media* **2015**, *110*. [CrossRef]
28. Krishna, R.; van Baten, J.M. Investigating the validity of the Bosanquet formula for estimation of diffusivities in mesopores. *Chem. Eng. Sci.* **2012**, *69*, 684–688. [CrossRef]
29. Thomas, H.C. Heterogeneous Ion Exchange in a Flowing System. *J. Am. Chem. Soc.* **1944**, *66*, 1664–1666. [CrossRef]
30. Afroze, S.; Sen, T.K.; Ang, H.M. Adsorption performance of continuous fixed bed column for the removal of methylene blue (MB) dye using Eucalyptus sheathiana bark biomass. *Res. Chem. Intermed.* **2016**, *42*, 2343–2364. [CrossRef]
31. Yoon, Y.H.; Nelson, J.H. Application of Gas Adsorption Kinetics I. A Theoretical Model for Respirator Cartridge Service Life. *Am. Ind. Hyg. Assoc. J.* **1984**, *45*, 509–516. [CrossRef] [PubMed]
32. El-Naas, M.H.; Alhaija, M.A.; Al-Zuhair, S. Evaluation of an activated carbon packed bed for the adsorption of phenols from petroleum refinery wastewater. *Environ. Sci. Pollut. Res.* **2017**, *24*, 7511–7520. [CrossRef]
33. Khalili, S.; Khoshandam, B.; Jahanshahi, M. A comparative study of CO_2 and CH_4 adsorption using activated carbon prepared from pine cone by phosphoric acid activation. *Korean J. Chem. Eng.* **2016**, *33*, 2943–2952. [CrossRef]
34. Romero-Pérez, A.; Aguilar-Armenta, G. Adsorption Kinetics and Equilibria of Carbon Dioxide, Ethylene, and Ethane on 4A(CECA) Zeolite. *J. Chem. Eng. Data* **2010**, *55*, 3625–3630. [CrossRef]
35. Harper, R.J.; Stifel, G.R.; Anderson, R.B. Adsorption of gases on 4A synthetic zeolite. *Can. J. Chem.* **1969**, *47*, 4661–4670. [CrossRef]
36. Wei, M.; Yu, Q.; Duan, W.; Hou, L.; Liu, K.; Qin, Q.; Liu, S.; Dai, J. Equilibrium and Kinetics Analysis of CO_2 Adsorption on Waste Ion-exchange Resin-based Activated Carbon. *J. Taiwan Inst. Chem. Eng.* **2017**, *77*, 161–167. [CrossRef]
37. Golchoobi, A.; Pahlavanzadeh, H. Molecular simulation, experiments and modelling of single adsorption capacity of 4A molecular sieve for CO_2–CH_4 separation. *Sep. Sci. Technol.* **2016**, *51*, 2318–2325. [CrossRef]
38. Mofarahi, M.; Gholipour, F. Gas adsorption separation of CO_2/CH_4 system using zeolite 5A. *Microporous Mesoporous Mater.* **2014**, *200*, 1–10. [CrossRef]
39. Wu, Y.-J.; Yang, Y.; Kong, X.-M.; Li, P.; Yu, J.-G.; Ribeiro, A.M.; Rodrigues, A.E. Adsorption of Pure and Binary CO_2, CH_4, and N_2 Gas Components on Activated Carbon Beads. *J. Chem. Eng. Data* **2015**, *60*, 2684–2693. [CrossRef]
40. Cornelius, M.-L.U.; Price, L.; Wells, S.A.; Petrik, L.F.; Sartbaeva, A. The steric influence of extra-framework cations on framework flexibility: An LTA case study. *Z. Krist. Cryst. Mater.* **2019**, *234*, 461–468. [CrossRef]
41. Rzepka, P.; Bacsik, Z.; Smeets, S.; Hansen, T.C.; Hedin, N.; Wardecki, D. Site-Specific Adsorption of CO_2 in Zeolite NaK-A. *J. Phys. Chem. C* **2018**, *122*, 27005–27015. [CrossRef]
42. Grajciar, L.; Čejka, J.; Zukal, A.; Areán, C.O.; Palomino, G.T.; Nachtigall, P. Controlling the Adsorption Enthalpy of CO_2 in Zeolites by Framework Topology and Composition. *ChemSusChem* **2012**, *5*, 2011–2022. [CrossRef] [PubMed]
43. Zukal, A.; Arean, C.O.; Delgado, M.R.; Nachtigall, P.; Pulido, A.; Mayerová, J.; Čejka, J. Combined volumetric, infrared spectroscopic and theoretical investigation of CO_2 adsorption on Na-A zeolite. *Microporous Mesoporous Mater.* **2011**, *146*, 97–105. [CrossRef]
44. Abdul Kareem, F.A.; Shariff, A.M.; Ullah, S.; Mellon, N.; Keong, L.K. Adsorption of pure and predicted binary (CO_2:CH_4) mixtures on 13X-Zeolite: Equilibrium and kinetic properties at offshore conditions. *Microporous Mesoporous Mater.* **2018**, *267*, 221–234. [CrossRef]
45. Pino, D.; Bessières, D. CH_4 /CO_2 Mixture Adsorption on a Characterized Activated Carbon. *J. Chem. Eng. Data* **2017**, *62*. [CrossRef]
46. Zhou, F.; Le-Hussain, F.; Guo, Z.; Yanici, S.; Cinar, Y. Adsorption/desorption characteristics for methane, nitrogen and carbon dioxide of coal samples from Southeast Qinshui Basin, China. *Energy Explor. Exploit.* **2013**, *31*, 645–666. [CrossRef]
47. Cheung, O.; Hedin, N. ChemInform Abstract: Zeolites and Related Sorbents with Narrow Pores for CO_2 Separation from Flue Gas. *ChemInform* **2014**, *45*. [CrossRef]
48. Rios, R.B.; Stragliotto, F.M.; Peixoto, H.R.; Torres, A.E.B.; Bastos-Neto, M.; Azevedo, D.C.S.; Cavalcante, C.L., Jr. Studies on the adsorption behavior of CO_2-CH_4 mixtures using activated carbon. *Braz. J. Chem. Eng.* **2013**, *30*, 939–951. [CrossRef]
49. Khalili, S.; Ghoreyshi, A.A.; Jahanshahi, M.; Khoshandam, B. Predictions of the adsorption equilibrium of CO_2/O_2 mixture on multi-walled carbon nanotube using Ideal Adsorbed Solution Theory. *J. Water Environ. Nanotechnol.* **2016**, *1*, 9–17. [CrossRef]
50. Singh, V.K.; Kumar, E.A. Comparative Studies on CO_2 Adsorption Kinetics by Solid Adsorbents. *Energy Procedia* **2016**, *90*, 316–325. [CrossRef]
51. Malekbala, M.; Soltani, S.; Abdul Rashid, S.; Luqman Chuah, A.; Rashid, U.; Imededdine, N.; Choong, T.; Teo, S.H. Optimization the Process of Chemically Modified Carbon Nanofiber Coated Monolith via Response Surface Methodology for CO_2 Capture. *Materials* **2020**, *13*, 1775. [CrossRef] [PubMed]

52. Gomez, L.; Zacharia, R.; Bénard, P.; Chahine, R. Simulation of binary CO_2/CH_4 mixture breakthrough profiles in MIL-53(Al). *J. Nanomater.* **2015**. [CrossRef]
53. Pino, L.; Italiano, C.; Vita, A.; Fabiano, C.; Recupero, V. Sorbents with high efficiency for CO_2 capture based on amines-supported carbon for biogas upgrading. *J. Environ. Sci.* **2016**, *48*, 138–150. [CrossRef]
54. Ahn, H.; Moon, J.-H.; Hyun, S.-H.; Lee, C.-H. Diffusion Mechanism of Carbon Dioxide in Zeolite 4A and CaX Pellets. *Adsorption* **2004**, *10*, 111–128. [CrossRef]
55. Arefi Pour, A.; Sharifnia, S.; Neishabori Salehi, R.; Ghodrati, M. Adsorption separation of CO_2/CH_4 on the synthesized NaA zeolite shaped with montmorillonite clay in natural gas purification process. *J. Nat. Gas. Sci. Eng.* **2016**, *36*, 630–643. [CrossRef]
56. Tobarameekul, P.; Sangsuradet, S.; Chat, N.; Worathanakul, P. Enhancement of CO_2 Adsorption Containing Zinc-ion-exchanged Zeolite NaA Synthesized from Rice Husk Ash. *Appl. Sci. Eng. Prog.* **2020**. [CrossRef]